Materials Research. 2023; 26(suppl. 1) : e20230074
DOI: https://doi.org/10.1590/1980-5373-MR-2023-0074

Effect of Hot Isostatic Pressing of Water Atomized AISI 316L Manufactured by Laser Powder Bed Fusion

Pedro Henrique Eça Rodrigues[a], Luiz Fernando Kultz Unti[a], Fábio Edson Mariani[a]*, Piter Gargarella[b], Osvaldo Mitsuyuki Cintho[c], Antonio J. Ramirez[d], Kahl Zilnyk[a]

[a]Instituto Tecnológico de Aeronáutica (ITA), Departamento de Materiais e Processos, São José dos Campos, SP, Brasil.
[b]Universidade Federal de São Carlos (UFSCar), Departamento de Engenharia de Materiais, São Carlos, SP, Brasil.
[c]Universidade Estadual de Ponta Grossa (UEPG), Departamento de Engenharia de Materiais, Ponta Grossa, PR, Brasil.
[d]Ohio State University (OSU), Department of Materials Science and Engineering, Columbus, OH, USA.

Received: January 16, 2023; Accepted: March 30, 2023

The objective of this work is to study the possibility of obtaining dense parts using water atomized AISI 316L steel powder in the L-PBF process. Despite its irregular, non-spherical, particle morphology, it has a significantly lower cost. 25 samples were produced varying the laser power and the scanning speeds to determine the optimal processing conditions. Additionally, hot isostatic pressing (HIP) was performed after the L-PBF process to further increase densification. Selected samples were subjected to microstructural characterization. The best densification results obtained were for the sample produced with the laser power of 173 W and scanning speed of 600 mm/s, where densifications close to 98% were obtained. HIP post-processing promoted increased densification of samples with closed porosity, allowing samples with densification above 95% to reach values close to 100%. HIP did not promote the closure of open pores. The results indicate that the use of water atomized AISI 316L in the L-PBF process combined with post-processing by HIP can produce dense engineering components and at the same time reduce the production costs of the manufactured components, mainly because it is a lower cost raw material when compared to the commonly used feedstock obtained by gas atomization.

Keywords: *Additive manufacturing, AISI 316L, water atomized powder, laser powder bed fusion, hot isostatic pressing.*

1. Introduction

Additive Manufacturing (AM) is developing rapidly due to the increasing need to produce customized parts or parts with complex geometries in industries as diverse as medical, dental, aerospace, nuclear and automotive[1-3]. Laser Powder Bed Fusion (L-PBF) is an AM process used to manufacture metal components with complex geometries, which allows to reduce post-fabrication operations[2,4]. The main process parameters are laser power, scanning speed, scanning strategy (XY axes), and layer thickness (Z axis). These parameters must be carefully selected to ensure minimal lack of fusion between the fabricated layers and to avoid keyhole induced porosities, defects which can influence the densification of the produced components[5]. The process allows constructional tolerances of approximately 50 µm and enables simultaneous manufacturing of multiple components during one operation[6]. However, there are limitations to the process, such as the low build rate, the need for unmelted powder removal, and the high cost of feedstock in the form of spherical powder (usually obtained by gas atomization)[5,7].

One possibility to reduce the L-PBF process cost and spread its use in industry is to optimize the process parameters to use more economical feedstocks. The water atomization process is commonly employed for the production of feedstock for sintered products, and it results in particles of irregular, non-spherical morphology[8]. The cost per ton of the water atomized powder is up to 10 times lower than the gas atomized, due to the production scale and the lack of expensive consumables such as argon gas[9].

AISI 316L austenitic stainless steel is one of the most widely used alloys in the L-PBF process due to its high corrosion resistance and good weldability, as well as one of the best materials used for structural finishing applications[10,11]. In the standard L-PBF process of AISI 316L stainless steel, the use of gas atomized powder as feedstock has been extensively explored[2,10,12,13]. On the other hand, the possibility of using a water atomized AISI 316L steel feedstock can reduce production costs. In view of this scenario, this work aims to characterize components produced by L-PBF process using water atomized AISI 316L stainless steel powder as feedstock. To obtain the best deposition conditions, a matrix of the process parameters was performed to identify the

*e-mail: mariani.fabioe@gmail.com

optimal processing window, which results in the best possible densification. Additionally, hot isostatic pressing (HIP) was performed after the L-PBF process to further increase the densification of the samples. Selected samples were subjected to microstructural characterization by optical and scanning electron microscopy, as well as X-ray diffraction. The results obtained were compared with results published in the literature for gas atomized AISI 316L stainless steel processed in the same L-PBF equipment[11].

2. Materials and Methods

The feedstock used in this work was water atomized AISI 316L powder (chemical composition in wt%: 17.00 Cr, 13.20 Ni, 2.40 Mo, 0.90 Si, 0.30 Mn, 0.03 C, and Fe balance) supplied by Brats - Sintered Filters Ind (Cajamar, Brazil). The flowability and apparent density of the powder were measured using a Hall flow meter, according to the standard ASTM B213[14]. Absolute density was also measured using a pycnometer. The particle size distribution (PSD) was measured by laser diffraction in a Panalytical Mastersizer 3000E equipment. The L-PBF deposition process was performed on an OmniSint-160 machine, manufactured by Omnitek Ind. (São Paulo, Brazil), equipped with a continuous-wave Nd:YAG fiber laser. To prevent the feedstock oxidation during processing, a high-purity argon atmosphere (99.997%) was used and the oxygen content in the manufacturing chamber was constantly monitored to be kept below 70 ppm.

25 samples (dimensions 10x10x5 mm^3) were produced varying the laser power (116, 147, 173, 190, and 226 W) and the scanning speeds (600, 450, 900, 1050, and 1200 mm/s) to determine the optimal processing conditions. The other process parameters were kept constant and were selected based on values already optimized for gas atomized AISI 316L powders[11]: layer thickness (30 µm), overlapping (80 µm), powder bed without prior heating, and bidirectional scanning strategy of 5 mm long strokes with 67° rotation between layers.

The volumetric energy density (VED - in unit J/mm^3) was calculated using the process parameters, according to Equation 1 and presented in Table 1, where P is the laser power (W), Vf is the laser scanning speed (mm/s), h is the overlapping ($80x10^{-3}$ mm), and t is the layer thickness ($30x10^{-3}$ mm).

$$VED = \frac{P}{Vf \times h \times t} \quad (1)$$

All samples were subjected to density measurement (densification) using the Archimedes' principle. For this purpose, the ASTM B311[15] standard was followed. Analytical grade ethanol was used instead of water to improve the samples wettability. Each sample was measured three times and the mean values were used to calculate the density according to Equation 2, where: dc: solid density (g/cm^3); dl: liquid density (g/cm^3); Ms: dry mass (g); and Mi: immersed mass (g).

$$dc = \left(\frac{Ms}{Ms - Mi} \right) \times dl \quad (2)$$

With the VED and densification results for each sample, an initial screening was carried out and some of the as-built samples were subjected to hot isostatic pressing (HIP) to evaluate the evolution in the densification and the microstructure. The HIP process was carried out in a QUINTUS QIH-15 equipment at 1100 °C for 3 hours in an 99,5% argon atmosphere at a pressure of 150 MPa, followed by furnace cooling.

Based on the densification values relative to the theoretical density of AISI 316L stainless steel (7.95 g/cm^3)[16], some samples were selected and sectioned using a low-speed metallographic cutter with a diamond disk, parallel to the construction direction, resulting in a 10x5 mm^2 section for analysis. The sectioned samples were mounted in bakelite, sanded on SiC sandpaper up to 2400 mesh grit, and polished on 0.3 µm alumina suspension.

Optical microscopy images were made on the polished surfaces for quantification and characterization of the samples porosity. Subsequently, the samples were electrolytic etched with a 40% (by volume) aqueous solution of HNO_3 at 1.1 V for a few seconds to reveal their microstructures. The microstructures were analyzed by optical and scanning electron microscopy (SEM). The SEM was also used to determine the chemical composition of the samples by energy dispersive X-ray spectroscopy (EDS). X-ray diffraction was also performed for phase quantification (austenite and ferrite) by Rietveld refinement using Panalytical Highscore Plus® software.

3. Results and Discussion

Figure 1 shows the particle size distribution with scanning electron micrographs (SEM) of the powder.

The distribution is mono-modal and is mostly between 15 and 45 µm, which is an ideal particle size range for the L-PBF process[5,10,11]. Particles show an irregular morphology, characteristic of the water atomization process[17,18]. The absolute density obtained by pycnometry was 7.67 ± 0.02 g/cm^3, lower than the theoretical density of AISI 316L stainless steel (7.95 g/cm^3)[16], indicating that the powder particles

Table 1. Parameter matrix (scanning speed and laser power) used.

Laser power (W)	Scanning speed (mm/s)				
	600	750	900	1050	1200
116	80.56	64.44	53.70	46.03	40.28
147	102.08	81.67	68.06	58.33	51.04
173	120.14	96.11	80.09	68.65	60.07
190	131.94	105.56	87.96	75.40	65.97
226	156.94	125.56	104.63	89.68	78.47

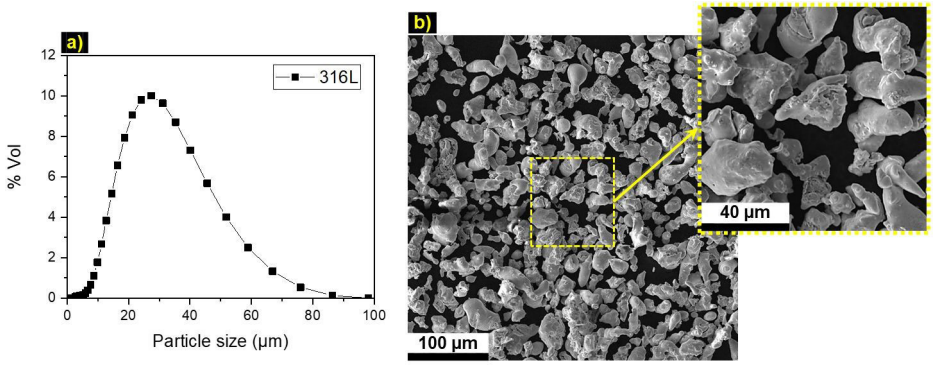

Figure 1. Water atomized AISI 316L powder: a) particle size distribution obtained by laser diffraction and b) SEM of particle morphology.

have internal porosity. Compared to a published study[10] for gas atomized AISI 316L powders with a similar particle size to those obtained in this work, the water atomized powder showed low fluidity (38 s in Hall Flow) and low relative density (3.31 g/cm^3). These results are due to the non-spherical morphology of the water atomized powder, which prevents a dense packing of the particles and impairs their flowability.

Figure 2 shows the results obtained for density using Archimedes' principle, according to ASTM B311[15], as a function of volumetric energy density (VED). It is observed that the three highest densification values, 98.58, 98.50, and 98.38%, were obtained for the samples produced with 173 W laser power. The highest densification obtained (98.58%) corresponds to the sample deposited with 120.14 J/mm^3 (173 W and 600 mm/s). The samples deposited with 116 W laser power, showed the three lowest densification values, 90.30, 92.57, and 94.53%, respectively. The lowest densification obtained (90.30%) corresponds to the sample deposited with 40.28 J/mm^3 (116 W and 1200 mm/s), the lowest VED analyzed. A comparison between this data with results published in the literature for gas atomized AISI 316L stainless steel processed in the same L-PBF machine[11], show that the feedstock morphology (water atomized powder) strongly influenced the densification results, reducing the apparent density of the as-built samples.

For each used laser power, there is a tendency to increase the samples densification with increasing VED, until reaching a plateau of approximately constant density. This behavior was also observed in other studies of L-PBF process parameterization[11,19,20]. On the other hand, other studies have indicated that excessive increase in VED can produce gas trapped and keyhole defects and consequently decrease the densification of the deposited samples[18,21].

Figure 3 shows the XRD analysis results for the water atomized powder along with the as-built samples. High intensity peaks referring to the austenitic phase (Fe-γ, FCC) are observed in the powder, along with a small d-ferrite (Fe-δ, BCC) peak, corresponding to the crystallographic plane {011}. The fraction of d-ferrite in the water atomized powder was estimated to be 3.0%. Austenitic stainless steels with molybdenum have high tendencies for presenting d-ferrite, since they present a ferritic-austenitic mode of solidification, i.e. The first solid phase to form from the liquid in equilibrium conditions is the BCC d-ferrite phase[22].

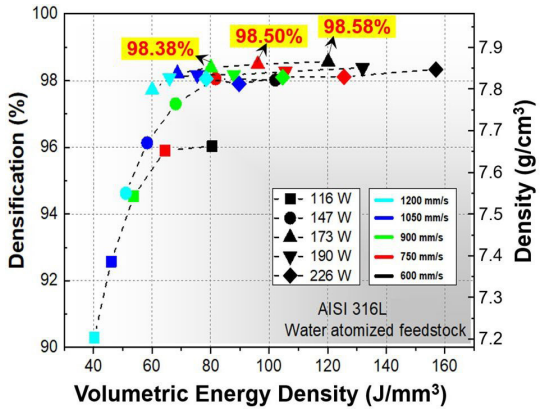

Figure 2. Density by means of Archimedes' principle (results in % and g/cm^3) as a function of volumetric energy density (VED).

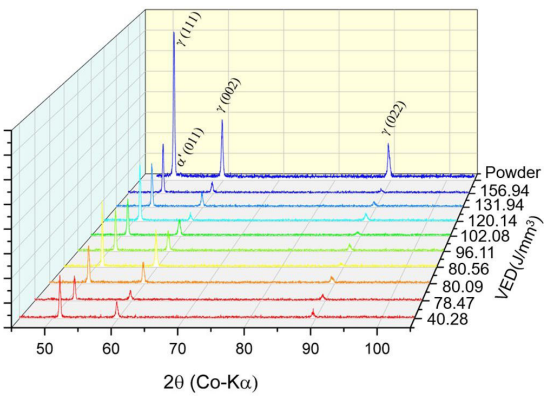

Figure 3. Graphical compilation of the results obtained by XRD.

In the L-PBF as-built samples, only peaks referring to the austenitic phase were observed. This single-phase structure is a product of the rapid cooling obtained after laser melting, which causes a large supercooling of the liquid that inhibits the formation of d-ferrite, ensuring that the manufactured samples kept only austenite as a present phase[11].

Figure 4 shows the densification results (using Archimedes' principle) after HIP post-processing, along with the densification

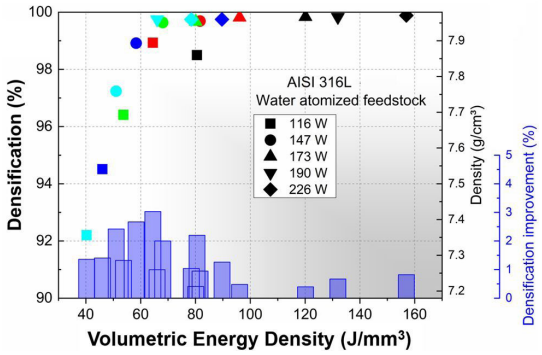

Figure 4. Densification results after HIP post-processing relative to VED.

improvement, relative to VED. The HIP post-processing promoted up to a 3% improvement in the densification of the deposited samples. Similar results were obtained in other studies that performed HIP process for L-PBF samples[23].

To efficiently analyze the process parameters studied, five samples were selected to be further characterized: the sample deposited with the highest densification before HIP post-processing (VED 120.14 J/mm³), and the samples deposited with minimum (40.28 J/mm³), intermediate (78.47 and 80.56 J/mm³) and maximum (156.94 J/mm³) VED used. In order to analyze whether the porosity obtained in the samples are open or closed types, the five selected samples were characterized using quantitative metallography by optical microscopy.

Figure 5 shows the optical micrographs of the cross sections from the five selected samples in the as-built and after HIP conditions. The densification results obtained by optical microscopy and Archimedes' principle methods are presented in Table 2.

In Figure 5a and 5c, for the as-built samples with 40.28, and 80.56 J/mm³, respectively, the presence of lack of fusion (predominant in the cross section) and gas trapped defects are observed. The lack of fusion comes from the insufficient heat input (116 W laser power) used that did not provide enough energy to complete melt the powder for any of the scanning speeds[11,16]. As the lack of fusion is a type of open porosity connecting the sample surface to its interior, the densification value obtained for this sample by means of the Archimedes' principle method diverged from the densification value obtained by quantitative metallography, which is more precise (Table 2). After HIP, it was observed that the lack of fusion remained, reducing only the gas trapped (closed porosity) defects. Due to this fact, no significant improvement in densification was obtained for these two samples after HIP.

For the as-built samples in Figure 5b, 5d, and 5e (VED: 78.47, 120.14, and 156.94 J/mm³, respectively), it is observed the presence of gas trapped and keyhole porosities. After HIP, it is noted that an increase in densification occurred, reaching values above 99% (Table 2), evidencing that post-processing has assisted in reducing these types of closed porosity. Similar results for closed porosity reduction were obtained in other published studies[19,20].

Figure 6 shows the scanning electron micrographs obtained on the samples deposited with VED of 40.28,

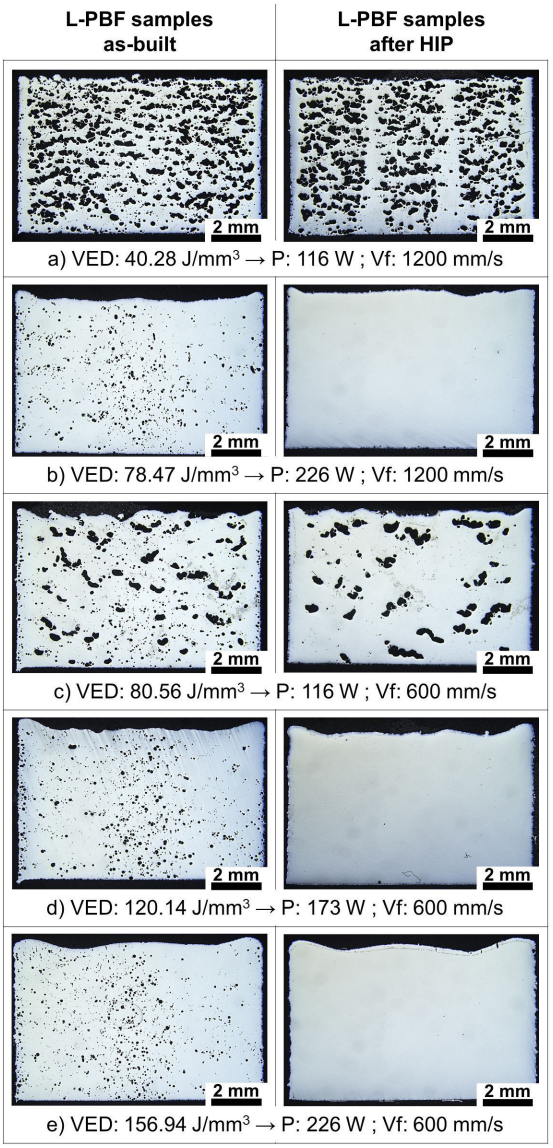

Figure 5. Optical micrographs of the cross sections of the five selected samples in the as-deposited and after HIP conditions. VED: a) 40.28, b) 78.47, c) 80.56, d) 120.14, and e) 156.94 J/mm³.

and 120.14 J/mm³, before HIP post-processing, showing the lack of fusion and gas trapped defects. For the sample deposited with VED of 40.28 J/mm³ (Figure 5a), unmelted powder particles are observed within the lack of fusion, evidencing that there was insufficient heat input. In both samples closed porosity (gas trapped) with a well-defined circumference is noted.

Figure 7 shows the melt pools depth (before HIP post-processing) in relation to the VED. The samples that presented the highest densification, indicated with the red arrows in Figure 7, are the ones that presented intermediate penetration depth values (between 70 and 115 µm), as well as more uniform geometric features (shallow and wide melt pools). These geometric uniformity characteristics difficult the appearance of lack of fusion defects, besides

Table 2. Comparison of densification results obtained for optical microscopy characterization and Archimedes' principle methods.

VED (J/mm³)	Archimedes' principle (%)		Optical microscopy characterization (%)	
	As-built	After HIP	As-built	After HIP
40.28	90.30	92.20	71.23	71.63
78.47	98.05	99.74	96.30	99.89
80.56	96.03	98.50	88.94	90.63
120.14	98.57	99.83	97.04	99.62
156.94	98.34	99.88	95.97	99.77

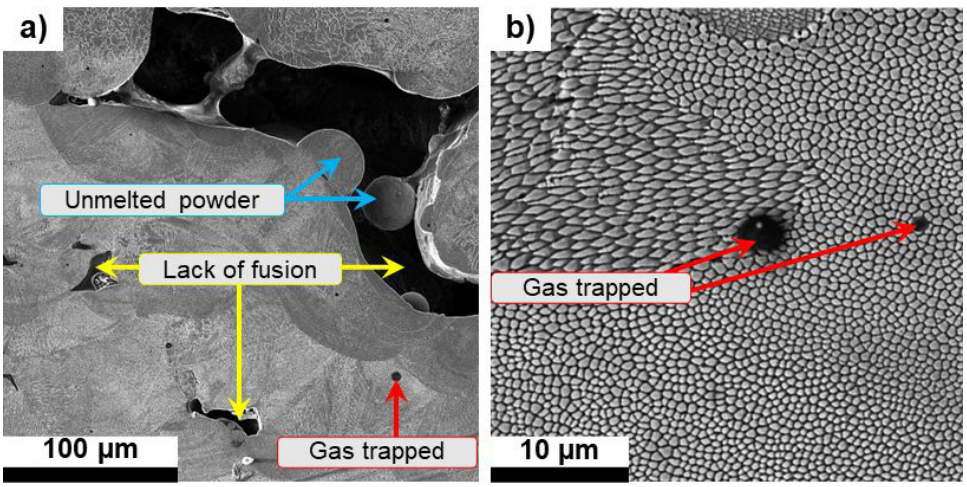

Figure 6. Scanning electron microscopy of the as-built samples: VED a) 40.28, and b) 120.14 J/mm³. Defects are indicated by red arrows (gas trapped) and yellow arrows (lack of fusion). Blue arrows indicate unmelted powder within the lack of fusion defect.

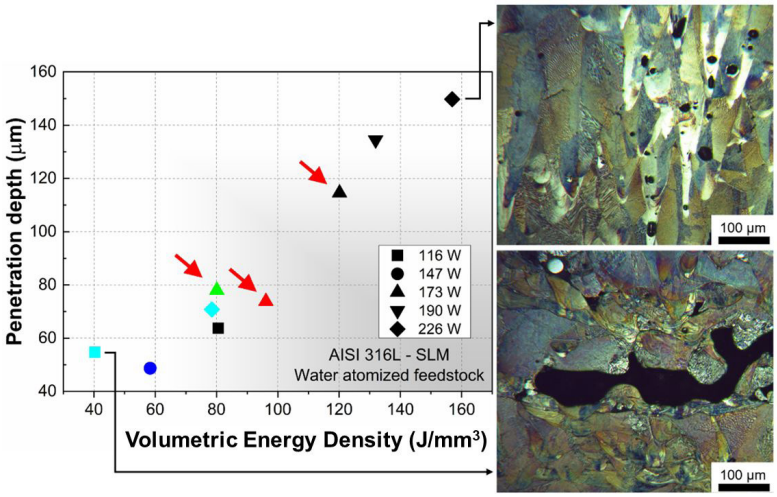

Figure 7. Melt pools depth in relation to the volumetric energy density (VED). Red arrows indicate the samples that showed the highest densification.

resulting in a lower presence of gas trapped of keyhole pores. However, for low values of VED the lack of fusion porosity directly interferes with densification. A similar trend emerges for high VED values, as observed in other works, since gas trapped and keyhole porosities are favored in such conditions[18,21].

Figure 8 shows the inverse pole figures (IPF) maps obtained from the EBSD analysis of as-built and after HIP samples. Both conditions presented virtually no preferred crystallographic orientation, but columnar grains aligned to the heat extraction direction are present on the as-built samples. However, HIP post-processing promoted the

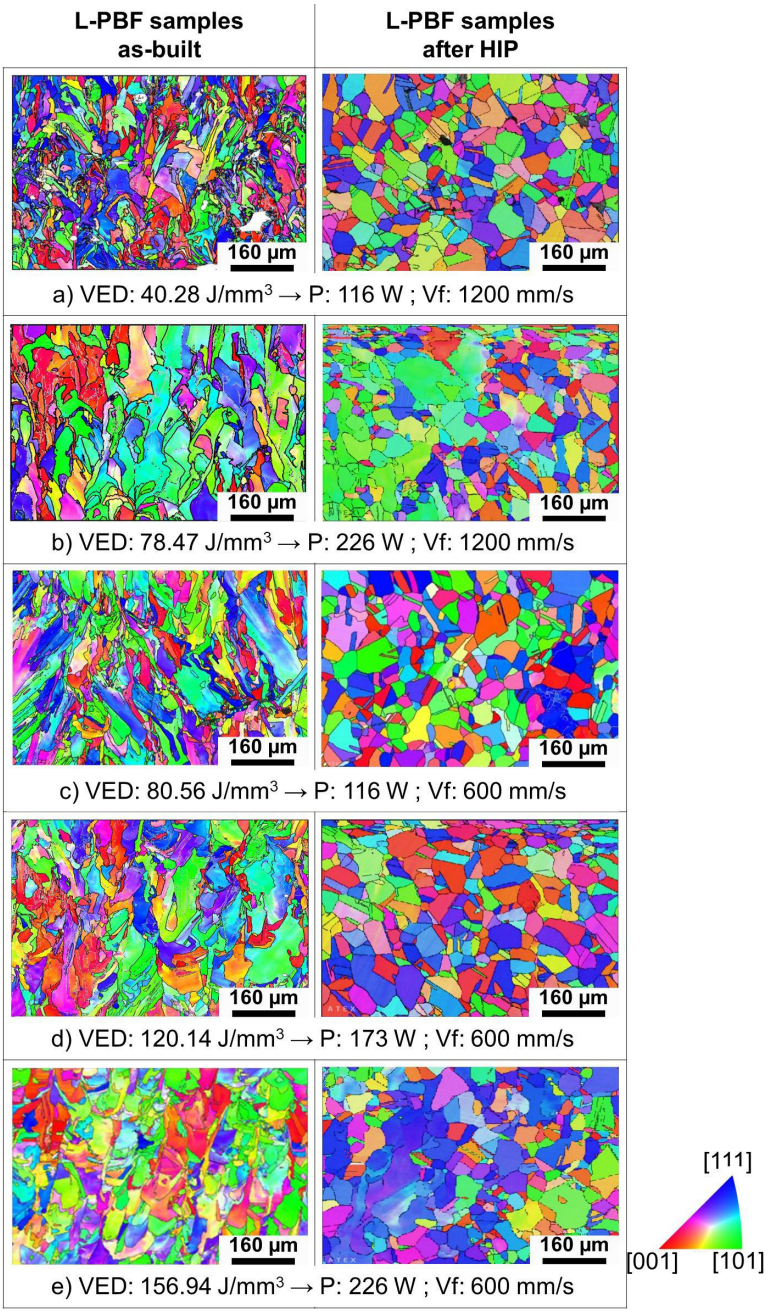

Figure 8. IPF maps of the five selected samples in the as-deposited and after HIP conditions. VED: a) 40.28, b) 78.47, c) 80.56, d) 120.14, and e) 156.94 J/mm³.

recrystallization of microstructures and equiaxed austenitic grains were obtained. This phenomime occurs due to the thermal cycling of the L-PBF process, which causes residual stresses and micro-deformations to build up in the microstructure, providing the necessary driving force for recrystallization to occur during the post-processing[12,13]. After HIP, the typical L-PBF columnar grains are no longer present, providing a more uniform and isotropic microstructure.

Finally, Figure 9 shows the ideal L-PBF processing window for water-sprayed 316L steel, for as-built and HIPed samples. Conditions that resulted in densifications above 98% according to the Archimedes principle and that did not show lack of fusion porosity or extensive keyhole formation in the optical microscopy analysis were considered approved. The HIP post-processing remarkably increased the number of approved processing conditions, including ones with higher scanning speed. This opens the possibility of not only using a cheaper feedstock, but also achieving shorter production times, helping to reduce the costs of fabrication by L-PBF and to spreading the industrial applications of this AM technology.

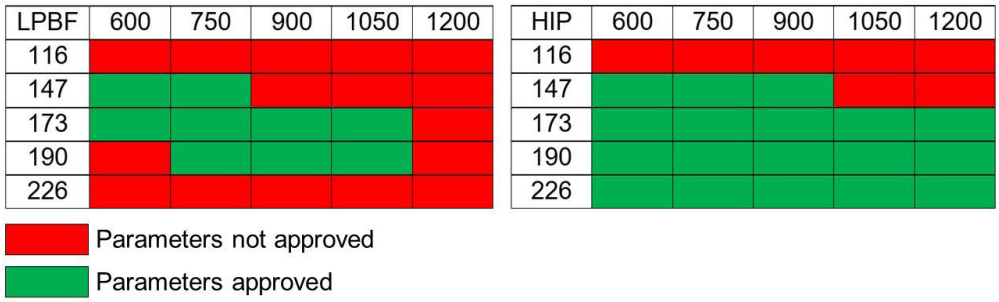

Figure 9. Optimal processing window for the water atomized 316L feedstock in the as-built condition (left) and after HIP (right). Red: parameters not approved. Green: parameters approved.

4. Conclusions

In this work, water atomized AISI 316L stainless steel powder were used as feedstock for sample depositions by L-PBF process. Subsequently, the deposited samples were subjected to HIP post-processing. The main findings from this study are summarized as follows:

- Water atomized AISI 316L stainless steel samples were deposited with densifications greater close to 98%. The best results were obtained with 173 W laser power and 600 mm/s scanning speeds, which are similar parameters to those used in the L-PBF process for the gas atomized feedstock.
- The HIP post-processing reduced the levels of closed porosities (gas trapped and keyhole), increasing the samples densification. However, the process was not able to reduce the open porosities (lack of fusion). Samples with densifications close to 95% had an increase of this property to values above 99% after HIP. This fact suggests that higher scanning speeds may be used in order to archive higher production without compromising the densification levels of the final component.
- The heat treatment (HIP) enabled microstructural recrystallization and erased the thermal history of the samples. This transformed the typical L-PBF microstructure (columnar grains growing parallel to the heat extraction direction) into fully-austenitic grains similar to the ones obtained by conventional manufacturing techniques.
- The results showed that the use of water atomized powder as a feedstock for L-PBF depositions when coupled with HIP post-processing has potential to produce dense engineering parts, which will allow the use of a low-cost feedstock, replacing the one obtained by gas atomization with higher production costs, thus reducing the expenses for the manufacturing of L-PBF components.

5. Acknowledgments

The authors gratefully acknowledge financial support from FAPESP (São Paulo Research Foundation) under grants 2019/06679-1 and 2017/27031-4, and laboratory support of CLABMU-UEPG. LFKU is thankful to CAPES (Coordination for the Improvement of Higher Education Personnel) for the PRINT scholarship and to CNPq (National Council for Scientific and Technological Development) for the financial support under grant 156279/2019-3. The authors are also indebted to 1st Ten. Eng. Natália Simões Evangelista and Dr. Adriana Medeiros Gama (AMR-IAE, Brazil) for their kind assistance with the HIP processing.

6. References

1. Huo YS, Hong C, Li HX, Liu P. Influence of different processing parameter on distortion and residual stress of inconel 718 alloys fabricated by selective laser melting (SLM). Mater Res. 2021;23(6):e20200176.
2. Bertoli US, Guss G, Wu S, Matthews MJ, Schoenung JM. In-situ characterization of laser-powder interaction and cooling rates through high-speed imaging of powder bed fusion additive manufacturing. Mater Des. 2017;135:385-96.
3. Santos C, Habibe AF, Simba BG, Lins JFC, Freitas BXD, Nunes CA. CoCrMo-base alloys for dental applications obtained by selective laser melting (slm) and cad/cam milling. Mater Res. 2020;23(2):e20190599.
4. Bomfim PKS, Coury FG, Wang P, Gargarella P. Characterization of AlCoCrFeNi high entropy alloy gas atomized powder. Mater Res. 2022;25:e20210120.
5. Fayazfar H, Salarian M, Rogalsky A, Sarker D, Russo P, Paserin V et al. A critical review of powder-based additive manufacturing of ferrous alloys: process parameters, microstructure and mechanical properties. Mater Des. 2018;144:98-128.
6. Niendorf T, Leuders S, Riemer A, Richard HA, Tröster T, Schwarze D. Highly anisotropic steel processed by selective laser melting. Metall Mater Trans, B, Process Metall Mater Proc Sci. 2013;44(4):794-6.
7. Bhavar V, Kattire P, Patil V, Khot S, Gujar K, Singh R. A review on powder bed fusion technology of metal additive manufacturing. In: Badiru AB, Valencia VV, Liu D, editors. Additive manufacturing handbook. 1st ed. Boca Raton: CRC Press; 2017. p. 251-3.
8. Pasebani S, Ghayoor M, Badwe S, Irrinki H, Atre SV. Effects of atomizing media and post processing on mechanical properties of 17-4 PH stainless steel manufactured via selective laser melting. Addit Manuf. 2018;22:127-37.
9. Fedina T, Sundqvist J, Powell J, Kaplan AF. A comparative study of water and gas atomized low alloy steel powders for additive manufacturing. Addit Manuf. 2020;36:101675.
10. Ziri S, Hor A, Mabru C. Combined effect of powder properties and process parameters on the density of 316L stainless steel obtained by laser powder bed fusion. Int J Adv Manuf Technol. 2022;120(9-10):6187-204.

11. Montuori RAM, Figueira G, Cataldi TP, Alcântara NGD, Bolfarini C, Coelho RT et al. Additive manufacturing of 316l stainless steel by selective laser melting. Soldag Insp. 2020;25:1-15.
12. Aota LS, Bajaj P, Zilnyk KD, Ponge D, Sandim HRZ. The origin of abnormal grain growth upon thermomechanical processing of laser powder-bed fusion alloys. Materialia. 2021;20:101243.
13. Aota LS, Bajaj P, Zilnyk KD, Jägle EA, Ponge D, Sandim HRZ et al. Recrystallization kinetics, mechanisms, and topology in alloys processed by laser powder-bed fusion: AISI 316L stainless steel as example. Materialia. 2021;20:101236.
14. ASTM International: American Society for Testing and Materials. ASTM B213: standard test methods for flow rate of metal powders using the carney funnel. West Conshohocken: ASTM International; 2017.
15. ASTM International: American Society for Testing and Materials. ASTM B311: test method for density determination for powder metallurgy (P/M) materials containing less. West Conshohocken: ASTM International; 2022.
16. Kurgan N. Effect of porosity and density on the mechanical and microstructural properties of sintered 316L stainless steel implant materials. Mater Des. 2014;55:235-41.
17. Haferkamp L, Haudenschild L, Spierings A, Wegener K, Riener K, Ziegelmeier S et al. The influence of particle shape, powder flowability, and powder layer density on part density in laser powder bed fusion. Metals. 2021;11(3):418.
18. Letenneur M, Brailovski V, Kreitcberg A, Paserin V, Bailon-Poujol I. Laser powder bed fusion of water-atomized iron-based powders: process optimization. J Manuf Mater Process. 2017;1(2):23.
19. Wang XJ, Zhang LC, Fang MH, Sercombe TB. The effect of atmosphere on the structure and properties of a selective laser melted Al–12Si alloy. Mater Sci Eng A. 2014;597:370-5.
20. Iveković A, Omidvari N, Vrancken B, Lietaert K, Thijs L, Vanmeensel K et al. Selective laser melting of tungsten and tungsten alloys. Int J Refract Met Hard Mater. 2018;72:27-32.
21. Jadhav SD, Dadbakhsh S, Goossens L, Kruth JP, Van Humbeeck J, Vanmeensel K. Influence of selective laser melting process parameters on texture evolution in pure copper. J Mater Process Technol. 2019;270:47-58.
22. Otubo J. A influência da ferrita delta em aços inoxidáveis austeníticos forjados. Rev Esc Minas. 2010;63(1):57-63.
23. Zhang M, Sun CN, Zhang X, Wei J, Hardacre D, Li H. High cycle fatigue and ratcheting interaction of laser powder bed fusion stainless steel 316L: fracture behaviour and stress-based modelling. Int J Fatigue. 2019;121:252-64.